Preprints (www.preprints.org) | NOT PEER-REVIEWED | Posted: 28 August 2020 doi:10.20944/preprints202008.0633.v1

Article

Maturation of pseudo-nucleus compartment in *P. aeruginosa*, infected with giant phiKZ phage

Yana A. Danilova [1], Viktoria V. Belousova [2], Andrey V. Moiseenko [1,3], Innokentii E. Vishnyakov [2,4], Maria V. Yakunina [2,5] and Olga S. Sokolova [1,6,*]

[1] Moscow Lomonosov University, Moscow, Russia
[2] Peter the Great St. Petersburg Polytechnic University, St. Petersburg, Russia
[3] Semenov Institute of Chemical Physics Russian Academy of Sciences, Moscow, Russia
[4] Institute of Cytology of the Russian Academy of Science, St. Petersburg, Russia
[5] Sechenov Institute of Evolutionary Physiology and Biochemistry Russian Academy of Sciences, St. Petersburg, Russia
[6] Shenzhen MSU-BIT University, Shenzhen, China
* Correspondence:Correspondence: sokolova@mail.bio.msu.ru; Tel.: +7-495-939-5738

Abstract: Bacteria develop various defense mechanisms against stresses, including the bacteriophage infection. The giant phiKZ phage infection induced the appearance of a pseudo-nucleus inside the bacterial cytoplasm. Here, we used FISH, electron tomography and analytical electron microscopy to study the morphology of this unique nucleus-like shell and to demonstrate the distribution of phiKZ and bacterial DNA in infected *P. aeruginosa* cells. The maturation of the pseudo-nucleus was traced in short intervals for 40 min after infection. This study was accompanied by the identification of phiKZ and bacterial DNA by real-time RCR. We demonstrated that phage DNA that isolated from the cytoplasm during all infection stages were compacted within the pseudo-nucleus in a specific structure. Bacterial DNA was diminished in the course of infection, but did not completely degrade until at least 40 min after phage application. The content of the total phage DNA, on the other hand, increased. EDX analysis confirmed these results and revealed that, during the infection, Sulfur content in the bacterial cytoplasm increased, which suggests the increase of DNA-binding Met-reach proteins synthesis, which could protect bacterial DNA from stress.

Keywords: giant phage; phiKZ; *Pseudomonas aeruginosa*; nucleoid; pseudo-nucleus; analytical electron microscopy; electron tomography; fluorescent *in situ* hybridization; stress response

1. Introduction

Giant phiKZ-like bacteriophages of the Myoviridae family, which include: *Pseudomonas aeruginosa* phiKZ, EL, OBP and *Pseudomonas chlororaphis* 201phi2-1, possess circular genetic maps [1,2] packaged inside the capsid according to the head-full mechanism. This means that, in the course of DNA packaging, the entire interior space of the head is filled with DNA. Sequencing of the giant phage genome revealed that the genome encodes not only the structural proteins of the phage capsid and tail, but also RNA polymerases [3,4], chaperonins [1,5] and proteins of the inner body [6]. The inner body is the internal proteinaceous structure, covered with genomic DNA [7]. It was discovered to be specific for giant phages [8,9]. The function of the inner body is to support the DNA inside the capsid, to participate in the genome injection to the bacterial cell, and to form the depo of phage proteins [6]. During injection of DNA into host cell, certain proteins are co-injected to build the machinery necessary for the transcription of early genes [6].

P. aeruginosa is a gram-negative, rod-shaped bacteria that causes severe diseases in animals, including humans [10,11]. Infection by *P. aeruginosa* often leads to generalized inflammation and sepsis and may cause fatal conditions [12], including morbidity and mortality in cystic fibrosis patients [13]. It is the second most common pathogen responsible for hospital-acquired bacterial

© 2020 by the author(s). Distributed under a Creative Commons CC BY license.

Preprints (www.preprints.org) | NOT PEER-REVIEWED | Posted: 28 August 2020 doi:10.20944/preprints202008.0633.v1

pneumonia [14]. Recently, the problem of bacterial resistance to antibiotics was highlighted by the World Health Organization (WHO), that has built up a catalogue of 12 families of bacteria that pose the greatest impact to human health, where *P. aeruginosa* was included as part of the most critical group [15]. Bacterial infections could be effectively withstood using phage therapy [16,17]. Phage treatment has shown to be substantially successful in comparison with monotherapy [18].

Bacteria develop various defense mechanisms against a bacteriophage infection. These include: blocking of phage receptors, production of an extracellular matrix and the production of competitive inhibitors to prevent phage absorption; superinfection exclusion (Sie); destroying foreign DNA with the Restriction-Modification system [19–21]; degradation of phage genetic material and building up inheritable DNA-encoded immunity ensured by clustered regularly interspaced short palindromic repeats (CRISPR) and CRISPR-associated (Cas) proteins from phage [19,22]. Meanwhile, bacteria react differently in response to phage predation [23]. The variety of responses is explained by the diversity of genetic features of a specific bacteriophage. For example, *S. enterica* engages a SOS response to lytic infection [24], while the response of *L. lactis* involves the induction of membrane stress proteins, d-alanylation of the cell wall and maintenance of the proton motive force (PMF) [23,25,26].

In its turn, the resistance of several phiKZ-like phages to bacterial defense systems, which is based on a double-stranded DNA cleavage, has recently been demonstrated [21]. It is intriguing how in the middle of the phage-infected bacterial cell an irregularly shaped nucleus-like compartment is formed, which is held in place with a bipolar tubulin spindle [21,27,28]. The shell of the compartment is believed to secure phage genomes from bacterial enzymes that are capable of cleaving phage DNA *in vitro* [21]. Apparently, the mRNA transcripts are translocated from the pseudo-nucleus to the cytoplasm for phage protein translation by ribosomes, similar to eukaryotic cells. Therefore, phage proteins associated with DNA replication or transcription are located in the bacterial cytoplasm [27].

Despite the apparent importance of this matter, the progress of understanding the maturation of the pseudo-nucleus and of the organization of DNA inside it has been mostly limited to fluorescent studies on live bacterial cells. Recently, structural studies of the infected cell's cytoplasm (i.e. outside the pseudo-nucleus) were performed, which revealed the newly assembled phage capsids docked to the contiguous shell of the pseudo-nucleus to be filled with the DNA [28]. So far, the spatial organization of the phage DNA inside the pseudo-nucleus shell eluded the attention of investigators.

Here, we used analytical electron microscopy, fluorescent *in situ* hybridization (FISH), real-time PCR and electron tomography to shed more light on the arrangement of unique nucleus-like shells and to demonstrate the distribution of phiKZ and bacterial DNA in the infected *P. aeruginosa* cells.

2. Materials and Methods

2.1. Bacteriophage, bacterial strain and growth conditions

The strain of *P. aeruginosa* PAO1 and phage phiKZ were generously donated by Dr V. Krylov (Mechnikov Research Institute of vaccines and sera). The PAO1 culture was grown in a LB medium at 37°C. High-titer phage phiKZ preparations were prepared from lysed infected PAO1 cultures and purified by centrifugation at 10,000 g for 10 minutes. To prepare infected cells for DNA extraction and EM-sample preparation, an overnight PAO1 culture was diluted 1:100 in 1 liter of fresh LB medium and, if it was needed, after reaching OD600 of 0.6 was infected with phiKZ at the multiplicity of infection of 10 (i.e. 10 phages to 1 bacteria cell). In some cases, 100 ug/ml of rifampicin was added to PAO1 5 min before the infection started. Cells were allowed to grow and the infection to spread until indicated time points and terminated by the addition of 100 ug/ml chloramphenicol and rapid cooling on an ice water bath. For further DNA extraction cells were harvested by centrifugation (5,000 g for 10 minutes), flash-frozen and stored at -20 °C until use. The preparation of the samples for EM will be described in the relevant section. The efficiency of infection was checked by determining the number of remaining colonies forming units in aliquots of infected cultures collected 5 minutes post-infection. Only cultures that contained less than 20% of surviving cells were used for further processing.

Preprints (www.preprints.org) | NOT PEER-REVIEWED | Posted: 28 August 2020 doi:10.20944/preprints202008.0633.v1

2.2. DNA extraction, agarose electrophoresis and real-time PCR

The DNA was extracted from bacteriophage particles using the standard phenol-chloroform extraction protocol. A GeneJet Genomic DNA Purification kit (TFS) was used to extract the DNA from infected and uninfected PAO1 cells. Equal quantities (400 ng) of total DNA from each sample were first treated with SmaI endonuclease (TFS) and then separated in 0,5% agarose gel using a low voltage (2-3 V/cm).

Real-time PCR analysis was performed on CFX96 Touch Real-Time PCR Detection System (Bio-Rad) using iTaq Universal SYBR Green Supermix (Bio-Rad) according to manufacturer's protocol. Pure bacterial and phage DNA in different concentrations (10, 5, 1 and 0.2 ng/ul) were used as standards. Samples of total DNA from infected cells were diluted to 10 ng/ul. Reactions for four standards and tree independent dilutions of each sample were performed simultaneously. The reaction without DNA was performed as negative controls in each series of dilutions. The following primers were used for bacterial and phage genomic DNA:

5′-TCTCTTTCGAGAGGTTGGC-3′ and 5′-TAACCCAGGGCGAGAAGTAC -3′ for a section of the bacterial RpoC gene

5′-GTGTATCATTTAGATAGC-3′ and 5′- GGTCATTGTGAAAGTAC-3′ for the late phage promotor P119L

CFX Maestro Software (Bio-Rad) was used for data analysis. The concentration of specific DNA in each reaction was calculated using standards. The resulting concentrations of specific DNAs in three independent dilutions of each sample were normalized against the total DNA concentration of 10 ng/ul, and the average fraction of bacterial and phage DNA for each sample was calculated. To estimate the error, the standard deviation was used.

2.3. Fluorescent in situ hybridization

Probes for PAO1 and phiKZ genomic DNA were made by digesting genomic DNA with sets of endonucleases (Hin1II, HaeIII, PstI, SphI for PAO1 DNA and Hin1II, HaeIII, HpaII, HindIII, XbaI, NdeI, NheI, NcoI, SphI, BglI for phiKZ DNA) and then labelling digested fragments with Cy5-dCTP using terminal deoxyribonucleotide transferase. PAO1 cells were grown in LB medium at 37°C until OD600=0.5-0.7, then cells were infected with phiKZ bacteriophage MOI=10. 750ul of cell culture before infection (0 min), after 15 and 30 min of infection were fixed with 4% paraformaldehyde and 0,1% glutaraldehyde for 30 min at room temperature, then centrifuged for 5 min at 2000g, resuspended in PBS and transferred to flow chamber slides treated with poly-L-lysine solution. Cells were left to adhere for 10 min at room temperature. Blocking solution (2XSSC buffer, 70% formamide, 1 mg/ml salmon sperm DNA) was applied and slides were heated at 75°C for 3 min. Slides were then washed with 70%, 90% and 96% ethanol for 5 minutes each at room temperature and dried. Cells were treated with 2xSSC, 50% formamide for 5 min at room temperature, then probes (200 ng/ul) were added in the same buffer. Cells were heated to 94°C for 3 min, then left at 42°C for 16 hours. Slides were washed with 2xSSC, 50% formamide at 37°C for 30 min twice, with 2xSSC, 25% formamide at room temperature for 10 min once, then with 2xSSC at room temperature 3 times, then once again with PBS. Total DNA was stained using DAPI. Shots were taken with the Nikon TI eclipse microscope; the Alexa647 channel was used for the Cy5 fluorophore, with exposure of 1000 ms, the DAPI channel was used for DAPI staining with exposure of 5 ms.

2.4. Transmission electron microscopy

Samples of non-infected cells and phiKZ-infected cells after 5, 10, 15, 20, 30 and 40 min of infection were chemically fixed using glutaraldehyde (2.5%) for 30 min at room temperature. Cells were collected by centrifugation at 5000 g on 4˚C. Then, cell pellets were washed twice with sterile PBS, postfixed in 1% osmium tetroxide (Electron Microscopy Sciences) during 30 min at room temperature, and subjected to EMbed 812 Kit (Electron Microscopy Sciences) embedding, according to the manufacturer protocol with replacement of 100% Propylene Oxide with 100% Acetone. Thin sections were cut with a diamond knife (Diatome) on the ultramicrotome Ultratome III 8800 (LKB, Sweden), transferred to nickel grids (400 mesh, Merck), covered with collodion, 2% in Amyl Acetate

Preprints (www.preprints.org) | NOT PEER-REVIEWED | Posted: 28 August 2020 doi:10.20944/preprints202008.0633.v1

(Electron Microscopy Sciences). Sections were contrasted with gadolinium triacetate (Uranyl Acetate Alternative, TedPella). Electron microscopy studies were performed using Libra120 120 kV transmission electron microscope (CarlZeiss, Germany) at magnification 8000×-16000×.

2.5. Sample preparation for analytical electron microscopy and electron tomography

Samples of non-infected cells and phiKZ-infected cells after 15 and 30 min of infection were chemically fixed using a mixture of glutaraldehyde (0.1%) and formaldehyde (2%) for 30 min at room temperature. The cells were collected by centrifugation at 5000 g on 4°C. Then, cell pellets were washed twice with sterile PBS and subjected to LR White (Polyscience, Inc., USA) embedding, according to the manufacturer protocol. Thin sections were cut with a diamond knife (Diatome) on the ultramicrotomes Ultracut-UCT (Leica Microsystems), transferred to copper 200 mesh grids, covered with formvar (SPI, USA). Some sections were contrasted with lead citrate.

2.6. Electron tomography

Ultrathin sections were examined with transmission electron microscope JEM-2100 (Jeol, Japan) with accelerating voltage 200 kV. GIF Quantum ER energy filter with 20 eV energy slit was used to filter out inelastically scattered electrons. Images were recorded with a Ultrascan 1000FTXP CCD camera (Gatan, USA) at pixel size 0.83 nm. Tomograms were obtained using the SerialEM software [29]. The sample tilt range was set from -60° to +60° with a 2 degrees step. Series of images were aligned by Gatan Digital Micrograph (Gatan, USA). Tomograms have been reconstructed with the back-projection algorithm in IMOD 4.9. Rendering the 3D scheme and isosurfaces preparation were accomplished in IMOD 4.9 [30,31].

2.7. Energy Dispersive X-ray Spectroscopy (EDX)

X-ray spectra were collected with Oxford Instruments X-Max 80 mm^2 EDS detector in STEM mode and summed over the sample area with a total exposure over 600 live seconds each.

2.8. Electron Energy Loss Spectroscopy (EELS)

EELS spectra and phosphorus elemental maps were obtained with the Gatan GIF Quantum ER spectrometer in STEM mode. Pixel size was set to 15-20 nm (varies from sample to sample). STEM drift correction was applied after each 40-50 pixels. Each spectrum was obtained at a 6.0 mrad collection angle, 0.25 eV dispersion and 132 eV energy shift. The spectra from different pixels were aligned to carbon K-edge.

During map processing, the background was fitted with power law over 115-128 eV energy range, which precedes phosphorus L2,3 edge, located at 132eV. Plural scattering effects were corrected using the Fourier-ratio deconvolution with the ZLP spectra taken from the same pixel array. The window for Phosphorus signal mapping was set to 132-172 eV.

3. Results

3.1. Maturation of the pseudo-nucleus in P.aeruginosa after phiKZ infection

To study the changes in the morphology of pseudo-nuclei over time after their infection, the cells were fixed before and 5-10-15-20-30-40 min after infection and embedded in resin by using the EMbed 812 Kit (Electron Microscopy Sciences), followed by ultrathin sectioning.

Preprints (www.preprints.org) | NOT PEER-REVIEWED | Posted: 28 August 2020 doi:10.20944/preprints202008.0633.v1

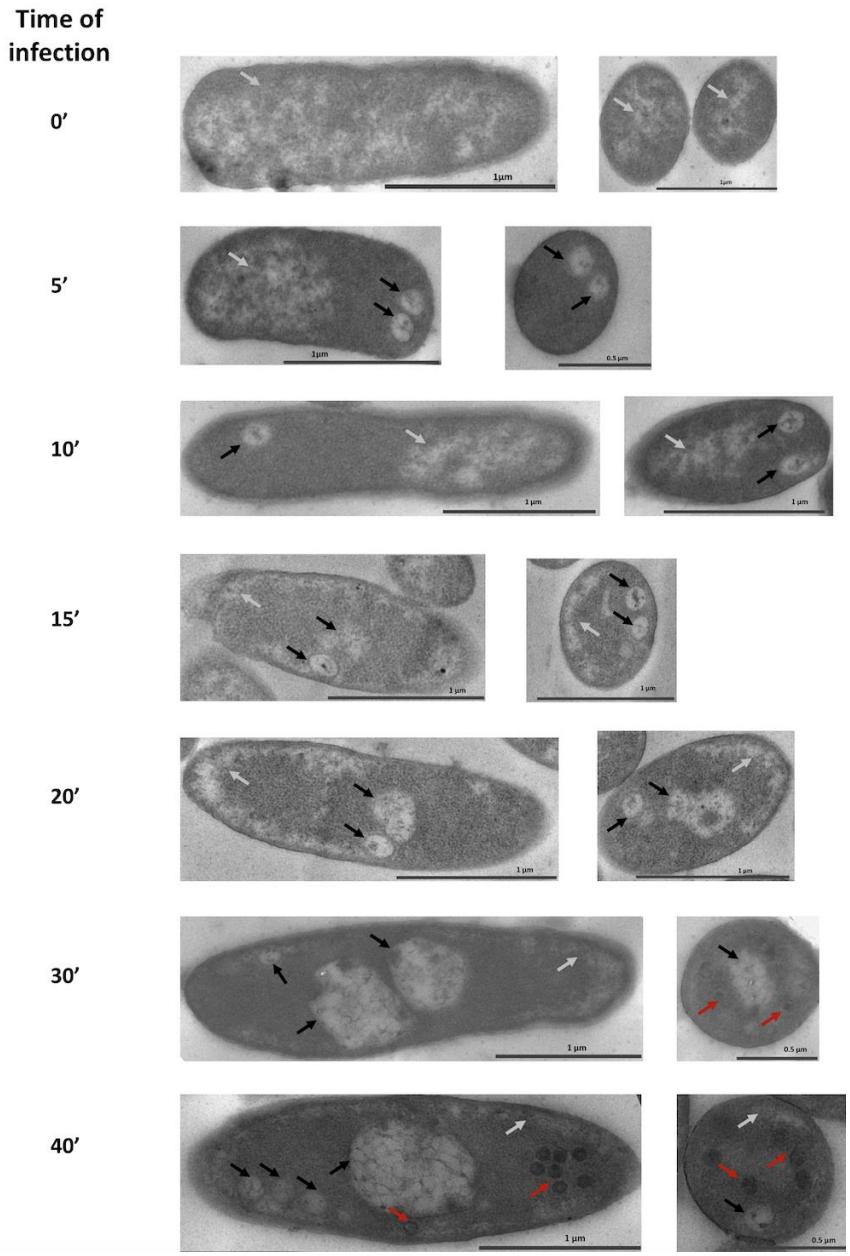

Figure 1. Time-course of the phiKZ infection and pseudo-nucleus maturation in *P. aeruginosa* cells. Left column - minutes after infection. White arrows – bacterial nucleoid; black arrows – RC and pseudo-nuclei at different stages of maturation; red arrows - new phage capsids.

In non-infected cells (0′ line on Fig. 1), the bacterial nucleoid and ribosomes were clearly visible. The nucleoid is diffused inside the cell with a tendency to occupy a central position; no pseudo-nucleus structure, nor any thresholds of the infection were detected (Fig. 1). The distribution of DNA in the cytoplasm of bacteria was estimated by EELS, the Phosphorus signal was detected and mapped onto the cell image (Fig. 2). All investigated cells contain the Phosphorus signal, but its spatial distribution differs depending on the post-infection time. In the non-infected cells, the Phosphorus signal was distributed evenly throughout the cytoplasm, reflecting the diffuse position of the nucleoid (Fig. 2c).

Preprints (www.preprints.org) | NOT PEER-REVIEWED | Posted: 28 August 2020 doi:10.20944/preprints202008.0633.v1

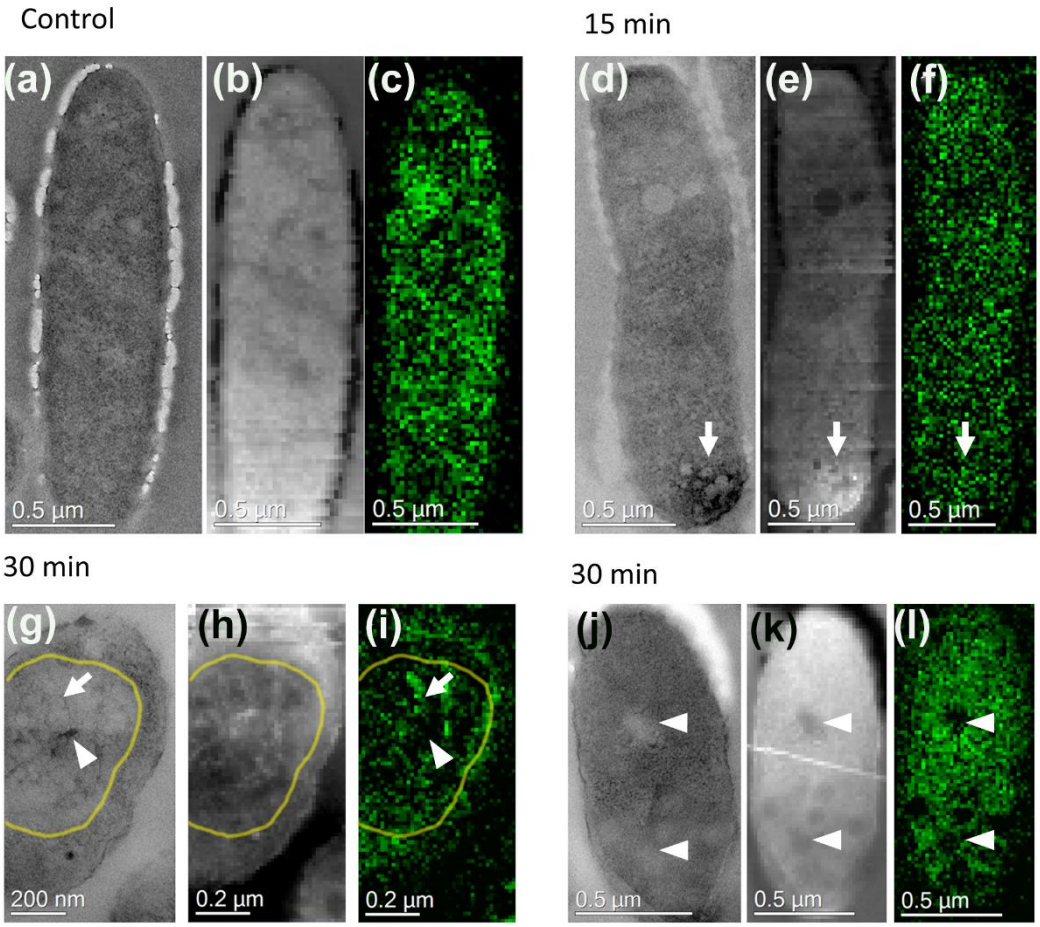

Figure 2. Phage and bacterial DNA distribution in control and infected *P. aeruginosa* cells. TEM image (a, d, g, j); HAADF image (b, e, h, k) and Phosphorus distribution maps through the pseudo-nucleus (c, f, i, l). P signal is mapped after background subtraction and multiple scattering correction with Fourier-ratio deconvolution. Arrows are pointing to the DNA-containing structures; arrowheads - to the areas, which do not contain the P signal; yellow outlines in (g, h, i) roughly mark the pseudo-nucleus border.

Upon the addition of phages to the cells, round compartments (RC) ~170 nm in diameter appeared after 5 min of infection close to the cell border. In some cells, more than one compartment was visible (Fig. 1). We suggested that the number of RC reflects the number of phages that attacked the cell, since we used the high multiplicity of infection to decrease the number of uninfected cells: ~10 phage particles per one bacterial cell (Fig. S1). These RC are separated from the cytoplasm and contain some electron-dense material (Fig. 1), which is, apparently, the proteinous remnants of the phiKZ inner body, subunits of phage RNAPs or chaperonins [6]. Moreover, after 5 min of infection, we observed the shift of the bacterial nucleoid to the cell pole opposite to the RC (Fig. 1). A similar displacement of the nucleoid continued until 10 min after infection. Up until the 15th min of infection, the bacterial nucleoid moves from the center of the cell to the periphery and occupies a submembrane position. The RC were kept in the cell, but, at the same time, in some cells we observed a new structure, which became more visible by the 20th min of infection. Such structures resembled a mature pseudo-nucleus, albeit smaller and with an underdeveloped internal network.

The even distribution of Phosphorus was detected in the cytoplasm at 15 min after infection (Fig. 2d-f); the overall intensity of the signal was higher comparing to control cells, while the small Sulfur peak appeared on the EDX spectrum (Fig. 3b). Since the Phosphorous signal has been present in RC with electron-dense material (Fig. 2d-f, arrows), we concluded that these compartments also contain nucleic acids.

Preprints (www.preprints.org) | NOT PEER-REVIEWED | Posted: 28 August 2020 doi:10.20944/preprints202008.0633.v1

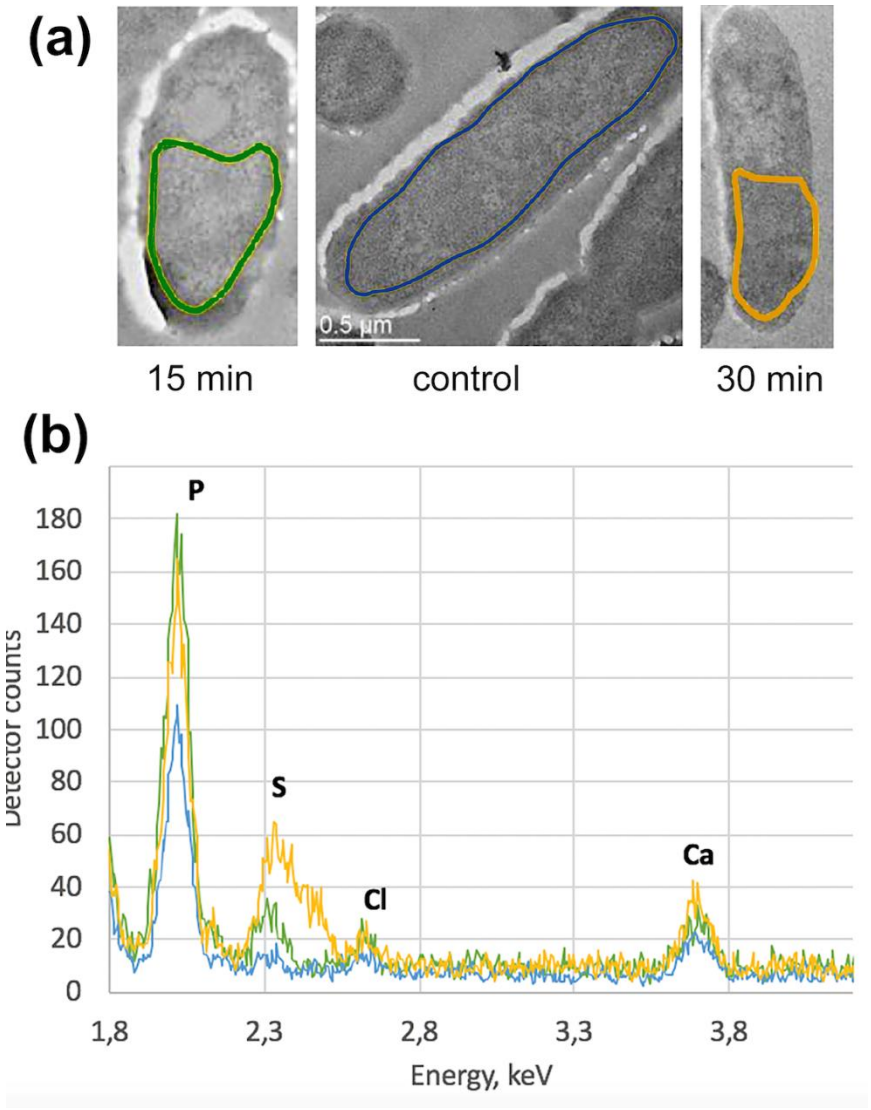

Figure 3. EDX spectra of *P. aeruginosa* control cells, 15 and 30 minutes after phiKZ infection. (a) Colored outlines mark the areas of bacteria, subjected for EDX analysis; (b) Superimposed EDX spectra from the selected areas, marked in (a), normalized to the C peak.

After 30 min of infection, the pseudo-nuclei maturated - they became almost spherical and were located close to the center of the cell (Fig. 1, 30'), similar to prior observations [21,28]. A single pseudo-nucleus was observed in ~88 % of infected cells, while the two-compartment pseudo-nucleus - in ~12 % of infected cells, in concordance with previous studies [28]. At the same time, in some cells the RC were still observed. The newly synthesized empty and filled phage capsids were detected both close to the surface of the pseudo-nucleus and to the cell wall (Fig. 1 and 6, Fig. S1). The average diameter of an empty capsid was 85 nm, a filled one – 100 nm, the latter somewhat smaller than the size of a phiKZ mature capsid, which is 145 nm [2,8,32], suggesting that the final maturation of the phage capsids is a future event. The bacterial nucleoid becomes less obvious at the periphery of the cell by the 40th min after the start of the infection, which could relate to the degradation of the bacterial DNA.

The distribution of the Phosphorous signal changes dramatically in cells infected for 30 min. We found that the pseudo-nuclei by the 30th min were filled with a branched network, whose distribution clearly corresponds to that of the Phosphorous (Fig. 2g-i), suggesting that it represents phage DNA. The empty capsids do not contain the Phosphorous signal, proving the lack of DNA (Fig. 2j-l). The bacterial cytoplasm was filled with an even Phosphorous signal, and its intensity was higher, comparing to the signal in control cells. The height of the Sulphur peak increased on the EDX spectrum (Fig. 3b).

Preprints (www.preprints.org) | NOT PEER-REVIEWED | Posted: 28 August 2020 doi:10.20944/preprints202008.0633.v1

3.2. Concentrations of phage and bacterial DNA switch in the course of phiKZ infection

To investigate deviations in bacterial and phage DNA concentration in the course of phage infection, we performed gel-electrophoresis and PCR analysis. Antibiotic rifampicin was added to the cell culture 5 min after phage addition to block the bacterial RNA polymerase, which stop the division of non-infected bacterial cells [33]. It was shown before that rifampicin does not influence the development of the phiKZ infection [34].

Total DNA samples were obtained from the non-infected and phiKZ-infected cells at the same time points as those in the morphological studies described above. To qualitatively assess the total DNA samples, agarose gel-electrophoresis was performed with preliminary cleavage of DNA by SmaI REase, which lacks the specific recognition sites in phage DNA, but cuts the bacterial genome into small fragments (less than 24 kbp each) (Fig. 4a).

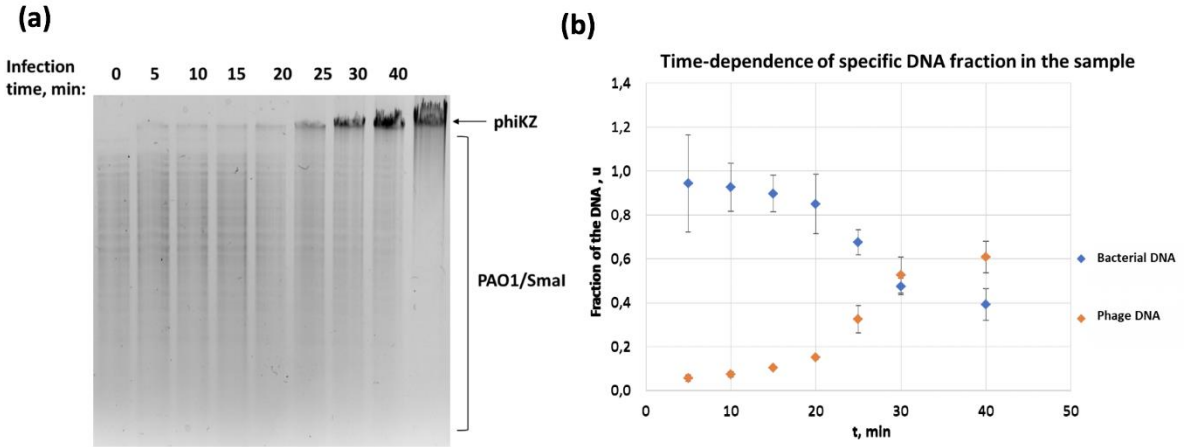

Figure 4. Analysis of the total DNA content from phiKZ-infected cells. (a) agarose gel-electrophoresis. Above the gel, the time points are mentioned, where '0' is a non-infected cell and the last line is the total DNA from phiKZ virions. PAO1/SmaI - DNA cleaved by SmaI REase. (b) real-time PCR. Filled circles - bacterial DNA, diamonds - phage DNA.

In the course of infection, the amount of phage DNA rapidly increased starting at 20 min after infection, while the bacterial DNA did not disappear completely and was still present at least up until the 40th min of infection. To refine these results, we conducted experiments to assess the ratio of phage/bacterial DNA at different time points after infection by real-time PCR. The plot in Fig. 4b shows an increase in the fraction of the bacteriophage genome and a decrease in the fraction of the bacterial genome, which starts after ~20 min of infection. Since the amount of total DNA for each point was the same, the observed effect is most likely associated with the onset of active replication of phage DNA, starting at the 20th min of infection. This is consistent with our gel electrophoresis results (Fig. 4a). However, it is difficult to draw a direct conclusion about what happens to bacterial DNA. To clarify this, we carried out an additional comparison of the theoretical and experimental mass ratio of the genomic phage DNA to the bacterium DNA at different time points after infection. As an internal control of the adequacy of our calculations and simplifications we analyze the mass ratio of the phage and bacterium DNA immediately after phage adsorption to the cell. To initiate the infection, at least one copy of the phage genome should enter the cell. At the onset of the infection, the mass ratio of phage DNA to bacterial DNA could be estimated as:

$$\frac{MW_{phiKZ} \cdot x}{MW_{PAO1}} \quad (1)$$

where MW_{phiKZ} and MW_{PAO1} are the molecular masses of the bacteriophage and bacterial genome, respectively, and x is the fraction of infected cells in the culture.

The comparison of the estimated values to the experimentally obtained values for two repetitions of the experiment (Table 1) revealed that the experimental values excess the estimated

Preprints (www.preprints.org) | NOT PEER-REVIEWED | Posted: 28 August 2020 doi:10.20944/preprints202008.0633.v1

ones by 1.7 - 2.5 times, which could be explained by the fact that, due to a 10-fold excess of phage particles over the number of cells in the culture, one cell can be attacked by more than one bacteriophage at a time, which is clearly seen on the micrographs (Fig. 1, 5′ and 10′; Fig. S1).

Table 1. Comparison of estimated values of the ratio of the phage DNA mass to bacterial DNA mass at 5 min after the infection starts.

Fraction of infected cells in culture, *x*	Estimated value of the DNAs mass ratio	Experimental value of the DNAs mass ratio
0.8	0.036	0.062
0.65	0.029	0.073

Up until the end of the infection cycle, about 100 new phiKZ phage particles are formed [7], which means that, at least by the end of the infection, there should be ~100 copies of the phage genome. We have shown that in the presence of rifampicin, which blocks further cell division in uninfected cells, the amount of bacterial DNA increased by 1.76 times in 40 min (Table 1S). If we assume that the bacterial DNA does not undergo degradation during infection and that the development of the bacteriophage does not prevent the completion of the bacterial genome replication, then the DNAs mass ratio can be theoretically calculated using the formula:

$$\frac{MW_{phiKZ} \cdot x \cdot 100}{MW_{PAO1} \cdot 1.76} \quad (2)$$

If we assume that the DNA of the bacterium in the infected cells is completely destroyed, then we will get another formula for calculating the DNAs ratio:

$$\frac{MW_{phiKZ} \cdot x \cdot 100}{MW_{PAO1} \cdot (1-x) \cdot 1.76} \quad (3)$$

Thus, we got two boundary values, which we compared with the experimental data (Table 2). The experimental values are 1.3 - 1.5 times less than the lower boundary of our assessment of the complete absence of bacterial DNA degradation. This means that the bacterial DNA does not undergo complete degradation in the case of infection of PAO1 cells with the phiKZ bacteriophage.

Table 2. Comparison of estimated values of the ration of the phage DNA mass to bacterial DNA mass at the end of the infection, AU.

Fraction of infected cells in culture, *x*	Estimated value of DNAs mass ratio without bacterial DNA degradation	Estimated value of DNAs mass ratio with full bacterial DNA degradation	Experimental value of DNAs mass ratio
0.8	2.03	10.17	1.55
0.65	1.65	4.72	0.97

3.3. Localization of bacterial and phage DNA during infection

To determine the intracellular localization of phage and bacterial DNA on the 15th and 30th min after infection time, we used FISH and specific Cy5-probes for bacterial and phage DNA, respectively (Fig. 5).

Preprints (www.preprints.org) | NOT PEER-REVIEWED | Posted: 28 August 2020 doi:10.20944/preprints202008.0633.v1

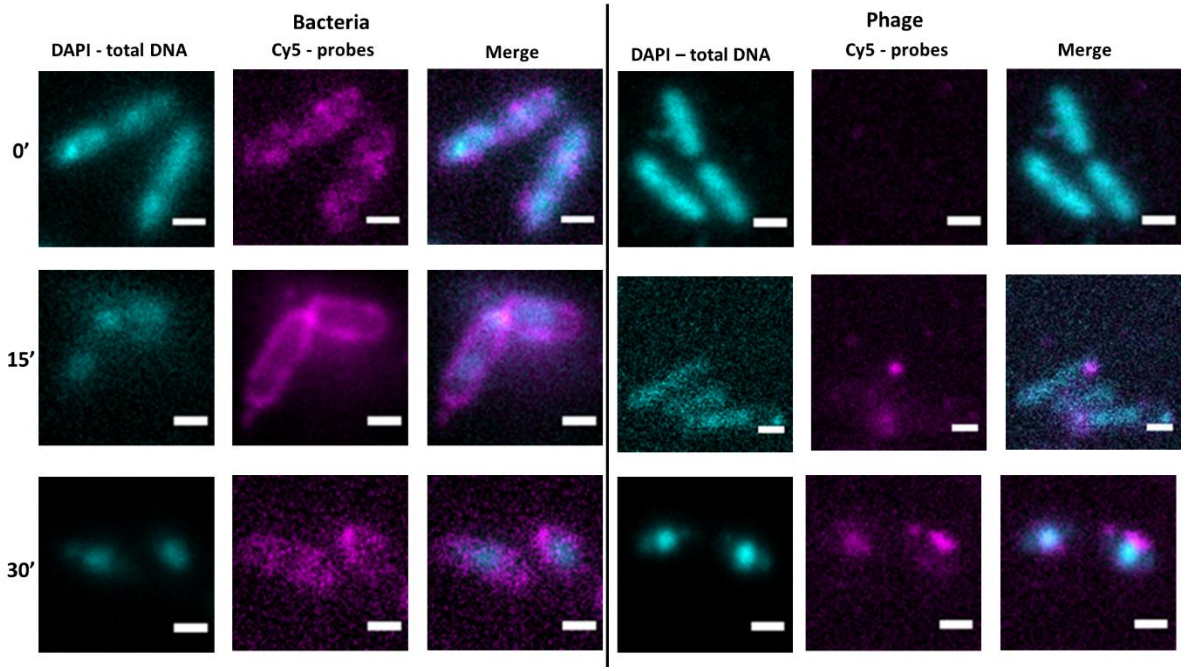

Figure 5. Analysis of bacterial and phage DNA at different times before and after infection of *P. aeruginosa* cells by the phiKZ phage. Time points are indicated on the left. Left part of the picture shows results of FISH with bacterial Cy5-probes, right part – with phage Cy5-probes. DAPI signal - cyan color, Cy5 signal is colored magenta. Bar – 1 um.

Non-infected cells were used as control; Fig. 5 demonstrates that in control cells the signal from the bacterial probes is diffusely located while phage probes did not hybridize with control cells. On the 15th min of infection, the signal for bacterial DNA shifted close to the cell membrane, corresponding with TEM data. The signal corresponded to the phage DNA revealed a condensed state, which may reflect RCs (bright magenta dots on the right side of Fig. 5) or early stages of pseudo-nucleus development (condense signals from DAPI on the left side of Fig. 5). Until the 30th min of infection, the phage DNA was localized in the center of the cell as a bright spherical spot reflecting the position of the pseudo-nucleus. At the same time, the bacterial DNA was diffusely spread within the cytoplasm.

3.4. 3D structure of the pseudo-nucleus

We used electron tomography to reveal the 3D structure of the DNA network inside the pseudo-nucleus (Fig. 6a, b). The infected cell at 30 min of infection possesses a mature pseudo-nucleus (Fig. 6a); we also detected some partially empty phage capsids (labeled 1 and 2), located close to the pseudo-nucleus border. The model obtained in IMOD [30,31] revealed about 90% of the network to be built by thin strands 2 or 4 nm thick (Fig. 6c), cross-linked with globular domains of ~10 nm of size. Considering that double-stranded DNA is ~2 nm thick [35], each filament, thus, consists of ~1-2 DNA double-helical strands (Fig. 6b, c). Thereby, the spatial structure of the pseudo-nucleus network (Fig. 6b) has been revealed.

Preprints (www.preprints.org) | NOT PEER-REVIEWED | Posted: 28 August 2020 doi:10.20944/preprints202008.0633.v1

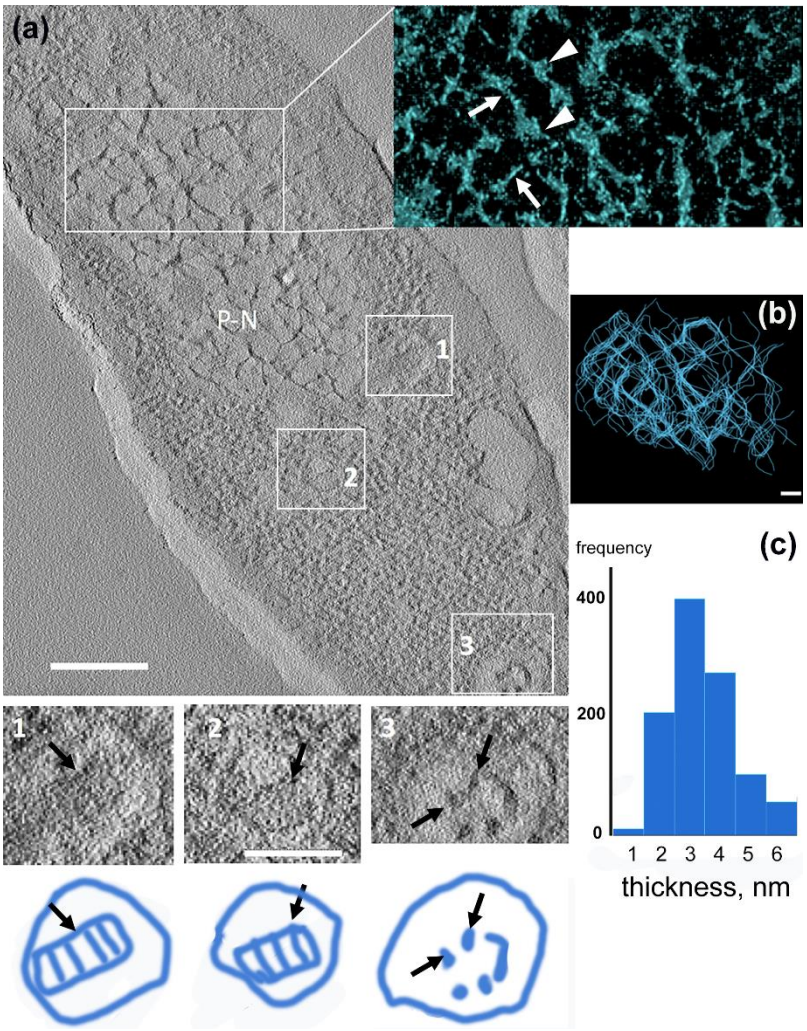

Figure 6. Electron tomography of a phiKZ infected *P. aeruginosa* cell. (a) A central slice through the tomogram of an infected cell (30 min after infection). Bar - 200 nm. P-N, pseudo-nucleus. Insert - 3D representation of P-N network. White arrows are pointing to DNA strands, arrowheads - to phage DNA-binding proteins. With #1 and #2 the phage capsids and corresponding gallery images are labeled. Bar size - 100 nm. Below each gallery image is the matching schematic of the capsid with the inner body marked with a black arrow; #3 and the corresponding gallery image represent a new phage entering the bacterial cell. The electron dense material is clearly visible inside the compartment (black arrows). (b) The subtomogram representation of the pseudo-nucleus network. Each blue strand represents one DNA helix. Bar - 50 nm. (c) The distribution (in %) of the average DNA strand's thickness in the pseudo-nucleus network.

Several newly formed capsids were visible close to the pseudo-nucleus border (two are marked on Fig. 5a by rectangles 1 and 2), which reveal icosahedral shapes with electron-dense cylinders inside (schematics #1 and #2). We think that these cylinders are the pre-formed inner bodies, which are a characteristic attribute of giant phages [8]. The average dimensions of these cylinders are about 40 nm x 90 nm, which corresponds well with the dimension of the phiKZ's inner body [8, 36].

4. Discussion

It was recently shown that phiKZ-like bacteriophages are resistant to many immune mechanisms of bacteria that normally target DNA *in vivo*, including two subtypes of CRISPR–Cas3, Cas9, Cas12a and restriction enzymes, such as HsdRMS and EcoRI [21]. These phenomena were excessively studied and linked to the appearance of a spherical compartment during phage infection in the bacterial cell. The formation of the spherical compartment was revealed using fluorescent microscopy [28,37] and electron tomography [28]. This compartment consists of a protein shell with

Preprints (www.preprints.org) | NOT PEER-REVIEWED | Posted: 28 August 2020 doi:10.20944/preprints202008.0633.v1

phage DNA on the inside. Some proteins that participate in transcription and replication of the phage genome were also found inside the shell. Thus, the compartment resembles the nucleus of a eukaryotic cell in its shape and phage DNA transcription-replication localization. Moreover, it was suggested that the walls of this compartment shield phage DNA from bacterial restriction enzymes and CRISPR nucleases. Here, we decided to focus on the fine structure of this pseudo-nucleus compartment and the DNA distribution inside and outside of it. We used transmission analytical electron microscopy and electron tomography to visualize the formation of the pseudo-nucleus structure in the *P. aeruginosa* cells subjected to the phiKZ infection.

To study the process of the maturation of the pseudo-nucleus compartment, we compared the size, location and contents of the compartments (Fig. 1) induced by phiKZ infection in the bacterial cell, as well as the DNA's concentration and localization (Fig. 4). 5 min after infection, intracellular RCs appeared close to the cell wall (Fig 1, 10′), likely marking the phage's entrance. Sometimes we observed two or more (Fig. 1S) such structures, which probably indicate a simultaneous attack of the cell by several phages, due to the high multiplicity of the infection. The RC were clearly separated from the cytoplasm, which suggests that they possess a shell. Some electron-dense material (Fig. 1) is visible inside these RC, which are, apparently, the proteinous remnants from the phiKZ virions. Since the phiKZ cell infection is resistant to bacterial defense systems from beginning to end [21], and the pseudo-nucleus does not form immediately, it can be assumed that the protection of the phage DNA at the beginning of infection is carried out by some proteins inside the RC. The mechanism of RC formation remains an intriguing question.

Within 15 min after infection, the variety of the intracellular compartment structures and shapes increased: in some cases, they resembled a pseudo-nucleus with a less developed network inside (Fig. 1, 15′, arrows), which reflects the graduate maturation of the pseudo-nucleus. A less developed internal network inside the 15th min non-mature pseudo-nucleus may reflect the active stage of phage DNA replication, which starts only by the 20th min of infection, according to the results of our electrophoretic analysis of total DNA preparations and RT-PCR (Fig. 4b). The diversity in the shapes of compartments may stem from a slightly different infection start point in each cell or from the cut planes that are passing through different parts of the cell. In the mature pseudo-nucleus, at the 30th min of infection, a saturated internal network of filaments was clearly visible; these filaments likely represent DNA bundles in complex with DNA-binding proteins. The presence of DNA in the bundles was confirmed by EELS (Fig. 2j). The genome size of the phiKZ phage is 280 kbp [2]; at the end of the infection there should be about 100 new phage particles [7] and, therefore, at least 100 copies of the phage genome should be located inside the pseudo-nucleus. Based on the indicated numbers, there should be about 28 Mbp of DNA inside the pseudo-nucleus, which implies the presence of a specific mechanism of phage DNA compactization. Perhaps, some phage proteins inside the pseudo-nucleus represent an analog of histones of the eukaryotic nucleus, which is in consistence with our observations of the globular domains of ~10 nm of size, binding to the double strain DNA (Fig. 6a, insert). Future biochemical and molecular biology studies are needed to identify the proteins inside the pseudo-nucleus.

During the process of phage infection, an unexpected distribution of the host nucleoid was revealed. From the 5th min of infection, the nucleoid changed its location inside the cell and shifted itself to cell poles to the opposite of the phage's entrance point. Until the 15th min after infection, it occupied a submembrane position, which was shown by TEM (Fig. 1) and FISH (Fig. 5) experiments. Later in the infection (30′ and 40′ on Fig. 1), the bacterial nucleoid disappeared from the submembrane position, however, according to the FISH results, its remnants remained in the cell until the 30th min of infection. It is interesting to note that, after phage infection, the amount of Phosphorus that reveals the DNA contents [38] increased in the bacterial cytoplasm according to EDX data (Fig. 3b). This may indicate a co-existence of both the phage DNA, whose content increased upon infection, and of the remaining host DNA (Fig. 4a). We performed PCR to check this hypothesis and demonstrated that the total amount of bacterial DNA, indeed, did not completely degrade until at least the 40th min of phage infection (Fig. 4b). These results are in contradiction with those presented by [37], for the related phage 201phi2-1 that infects *Pseudomonas chlororaphis*. Using FISH and

Preprints (www.preprints.org) | NOT PEER-REVIEWED | Posted: 28 August 2020 doi:10.20944/preprints202008.0633.v1

fluorescence microscopy, the authors reported the degradation of the host DNA by the 40th min of infection.

We proposed that the remaining host DNA may degrade slowly and be inaccessible for DNases, because it is bound to the host's stress proteins, like the DNA-binding protein from starved cells (Dps) [39–41], the synthesis of which generally increases in stress conditions. It is known that phage infection can elicit diverse stress responses in bacterial cells [23]. It has been shown to affect the regulation of specific stress proteins like the ones related to osmotic, nutrient and temperature stresses. For example, it was demonstrated that the folding of capsid proteins (P3 and P5) of coliphage PRD1 depends on proteins GroES and GroEL of *E. coli*, which are also responsible for heat shock protection [42]. It was suggested earlier that the giant phiKZ-like phages might directly change the metabolism of the bacterial cell to obtain subsequent support during phage maturation [43].

To check this hypothesis, we performed EDX analysis and detected a pronounced peak of Sulphur in the bacterial cytoplasm as early as on the 15th min of infection, while its size increased by the 30th min (Fig. 3b). This may indicate an increase in the content of Sulphur-containing proteins, like the above-mentioned Dps. Dps contains 48 Met per 24-mer, which possess enough Sulphur to be detected by X-ray spectroscopy [44]. The increasing contents of Dps leads to the increased protection of bacterial DNA. Notably, the pseudo-nucleus structure, visualized at 30 min in *P. aeruginosa*, closely resembles isotropic liquid crystalline DNA packaging (Fig. 2S), which is known to be the first stage of DNA protection against various stress factors in *E. coli* [38]. In liquid crystalline packaging, the DNA-Dps reduces the accessibility of DNA molecules to various external damaging factors, including irradiation, oxidizing agents, and external nucleases. We suggested that the formation of a pseudo-nucleus is a unique safety mechanism, originally developed in bacteria to protect its nucleoid from stress [41,45,46], which may be utilized in the course of evolution by bacteriophages for their needs. However, this hypothesis needs further investigation.

To summarize our results, we can suggest that the maturation of the pseudo-nucleus is a complex multi-stage process, connected to phage DNA replication and condensation. We have shown that the development of the phiKZ infection has a significant effect on the placement and structure of the bacterial nucleoid. Moreover, the unique packaging of the DNA inside the pseudo-nucleus or the preceding round compartments in the cytoplasm of the live bacterial cell is the main reason for infection sustainability of the phiKZ bacteriophage. The high-resolution structure of the liquid crystalline network is a subject for future research.

Supplementary Materials: The following are available online at www.mdpi.com/xxx/s1, **Table 1S**: Calculation of the coefficient reflecting the increase in the amount of extracted bacterial DNA during incubation of cells with the antibiotic rifampicin; **Figure 1S**: The empty phage particles attached to the phiKZ-infected cell. **Figure 2S**: Liquid crystalline DNA compactization in starved *E. coli* cell.

Author Contributions: Conceptualization, O.S.S. and M.V.Y.; investigation, Y.A.D., V.V.B., I.E.V. and A.V.M.; writing—original draft preparation, Y.A.D.; writing—review and editing, Y.A.D., O.S.S. and M.V.Y.; visualization, A.V.M, V.V.B.; funding acquisition, O.S.S. and M.V.Y. All authors have read and agreed to the published version of the manuscript.

Funding: The Electron tomography and analytical electron microscopy experiments were funded by RFBR (#19-04-00605 to O.S.S.). The DNA dynamics, FISH experiments and analysis of pseudo-nucleus formation by TEM were performed under support of RSF (#19-74-10030 to M.V.Y.).

Acknowledgments: Authors thank Dr Viktor Krylov for donation of phiKZ and Mrs. Lisa Trifonova for proofreading the manuscript. X-ray and EELS spectra and tomograms were obtained using the Unique equipment setup '3D-EMC' (supported by Ministry of science and higher education of Russian Federation, identifier #RFMEFI61919X0014).

Conflicts of Interest: The authors declare no conflict of interest.

References

1. Hertveldt, K.; Lavigne, R.; Pleteneva, E.; Sernova, N.; Kurochkina, L.; Korchevskii, R.; Robben, J.; Mesyanzhinov, V.; Krylov, V.N.; Volckaert, G. Genome Comparison of Pseudomonas aeruginosa Large Phages. *J. Mol. Biol.* **2005**, *354*, 536–545, doi:10.1016/j.jmb.2005.08.075.

Preprints (www.preprints.org) | NOT PEER-REVIEWED | Posted: 28 August 2020 doi:10.20944/preprints202008.0633.v1

2. Mesyanzhinov, V. V.; Robben, J.; Grymonprez, B.; Kostyuchenko, V.A.; Bourkaltseva, M. V.; Sykilinda, N.N.; Krylov, V.N.; Volckaert, G. The genome of bacteriophage φKZ of Pseudomonas aeruginosa. *J. Mol. Biol.* **2002**, *317*, 1–19, doi:10.1006/jmbi.2001.5396.
3. Ceyssens, P.-J.; Minakhin, L.; Van den Bossche, A.; Yakunina, M.; Klimuk, E.; Blasdel, B.; De Smet, J.; Noben, J.-P.; Blasi, U.; Severinov, K.; et al. Development of Giant Bacteriophage ϕKZ Is Independent of the Host Transcription Apparatus. *J. Virol.* **2014**, *88*, 10501–10510, doi:10.1128/JVI.01347-14.
4. Yakunina, M.; Artamonova, T.; Borukhov, S.; Makarova, K.S.; Severinov, K.; Minakhin, L. A non-canonical multisubunit RNA polymerase encoded by a giant bacteriophage. *Nucleic Acids Res.* **2015**, gkv1095, doi:10.1093/nar/gkv1095.
5. Lecoutere, E.; Ceyssens, P.-J.; Miroshnikov, K.A.; Mesyanzhinov, V. V.; Krylov, V.N.; Noben, J.-P.; Robben, J.; Hertveldt, K.; Volckaert, G.; Lavigne, R. Identification and comparative analysis of the structural proteomes of ϕKZ and EL, two giant Pseudomonas aeruginosa bacteriophages. *Proteomics* **2009**, *9*, 3215–3219, doi:10.1002/pmic.200800727.
6. Thomas, J.A.; Rolando, M.R.; Carroll, C.A.; Shen, P.S.; Belnap, D.M.; Weintraub, S.T.; Serwer, P.; Hardies, S.C. Characterization of Pseudomonas chlororaphis myovirus 201ϕ2-1 via genomic sequencing, mass spectrometry, and electron microscopy. *Virology* **2008**, *376*, 330–338, doi:10.1016/j.virol.2008.04.004.
7. Krylov, V.N.; Smirnova, T.A.; Minenkova, I.B.; Plotnikova, T.G.; Zhazikov, I.Z.; Khrenova, E.A. Pseudomonas bacteriophage contains an inner body in its capsid. *Can. J. Microbiol.* **1984**, *30*, 758–762, doi:10.1139/m84-116.
8. Sokolova, O.S.; Shaburova, O.V.; Pechnikova, E.V.; Shaytan, A.K.; Krylov, S.V.; Kiselev, N.A.; Krylov, V.N. Genome packaging in EL and Lin68, two giant phiKZ-like bacteriophages of P. aeruginosa. *Virology* **2014**, *468–470*, 472–478, doi:10.1016/j.virol.2014.09.002.
9. Matsko, N.; Klinov, D.; Manykin, A.; Demin, V.; Klimenko, S. Atomic force microscopy analysis of bacteriophages phiKZ and T4. *J. Electron Microsc. (Tokyo).* **2001**, *50*, 417–22, doi:10.1093/jmicro/50.5.417.
10. Wu, W.; Jin, Y.; Bai, F.; Jin, S. Pseudomonas aeruginosa. In *Molecular Medical Microbiology, 2nd ed.*; Elsevier, 2015; Vol. 2, pp. 753–767. ISBN 9780123971692.
11. Pier, G.B. Pseudomonas and Related Gram-Negative Bacillary Infections. In *Goldman's Cecil Medicine; 24th ed.*; Elsevier, 2012; Vol. 2, pp. 1877–1881. ISBN 9781437716047.
12. *Pseudomonas aeruginosa: infections and treatment.*; Baltch, A.L., Smith, R.P., Eds.; Marcel Dekker, Inc.: New York, USA, 1994.
13. Jones, R.N. Microbial Etiologies of Hospital-Acquired Bacterial Pneumonia and Ventilator-Associated Bacterial Pneumonia. *Clin. Infect. Dis.* **2010**, *51*, S81–S87, doi:10.1086/653053
14. Gómez, M.I.; Prince, A. Opportunistic infections in lung disease: Pseudomonas infections in cystic fibrosis. *Curr. Opin. Pharmacol.* **2007**, *7*, 244–251, doi:10.1016/j.coph.2006.12.005.
15. WHO publishes list of bacteria for which new antibiotics are urgently needed. Available online: https://www.who.int/news-room/detail/27-02-2017-who-publishes-list-of-bacteria-for-which-new-antibiotics-are-urgently-needed (accessed on Feb 23, 2020).
16. Burrowes, B.; Harper, D.R.; Anderson, J.; McConville, M.; Enright, M.C. Bacteriophage therapy: potential uses in the control of antibiotic-resistant pathogens. *Expert Rev. Anti. Infect. Ther.* **2011**, *9*, 775–785, doi:10.1586/eri.11.90.
17. Chang, R.Y.K.; Wallin, M.; Lin, Y.; Leung, S.S.Y.; Wang, H.; Morales, S.; Chan, H.-K. Phage therapy for respiratory infections. *Adv. Drug Deliv. Rev.* **2018**, *133*, 76–86, doi:10.1016/j.addr.2018.08.001.
18. Torres-Barceló, C.; Arias-Sánchez, F.I.; Vasse, M.; Ramsayer, J.; Kaltz, O.; Hochberg, M.E. A Window of Opportunity to Control the Bacterial Pathogen Pseudomonas aeruginosa Combining Antibiotics and Phages. *PLoS One* **2014**, *9*, e106628, doi:10.1371/journal.pone.0106628.
19. Labrie, S.J.; Samson, J.E.; Moineau, S. Bacteriophage resistance mechanisms. *Nat. Rev. Microbiol.* **2010**, *8*, 317–327, doi:10.1038/nrmicro2315.
20. Meselson, M.; Yuan, R.; Heywood, J. Restriction and Modification of DNA. *Annu. Rev. Biochem.* **1972**, *41*, 447–466, doi:10.1146/annurev.bi.41.070172.002311.
21. Mendoza, S.D.; Nieweglowska, E.S.; Govindarajan, S.; Leon, L.M.; Berry, J.D.; Tiwari, A.; Chaikeeratisak, V.; Pogliano, J.; Agard, D.A.; Bondy-Denomy, J. A bacteriophage nucleus-like compartment shields DNA from CRISPR nucleases. *Nature* **2020**, *577*, 244–248, doi:10.1038/s41586-019-1786-y.
22. Horvath, P.; Barrangou, R. CRISPR/Cas, the Immune System of Bacteria and Archaea. *Science* **2010**, *327*, 167–170, doi:10.1126/science.1179555.

Preprints (www.preprints.org) | NOT PEER-REVIEWED | Posted: 28 August 2020 doi:10.20944/preprints202008.0633.v1

23. Fernández, L.; Rodríguez, A.; García, P. Phage or foe: An insight into the impact of viral predation on microbial communities. *ISME J.* **2018**, *12*, 1171–1179, doi:10.1038/s41396-018-0049-5.
24. Campoy, S.; Hervàs, A.; Busquets, N.; Erill, I.; Teixidó, L.; Barbé, J. Induction of the SOS response by bacteriophage lytic development in Salmonella enterica. *Virology* **2006**, *351*, 360–367, doi:10.1016/j.virol.2006.04.001.
25. Fallico, V.; Ross, R.P.; Fitzgerald, G.F.; McAuliffe, O. Genetic Response to Bacteriophage Infection in Lactococcus lactis Reveals a Four-Strand Approach Involving Induction of Membrane Stress Proteins, D-Alanylation of the Cell Wall, Maintenance of Proton Motive Force, and Energy Conservation. *J. Virol.* **2011**, *85*, 12032–12042, doi:10.1128/JVI.00275-11.
26. Ainsworth, S.; Zomer, A.; Mahony, J.; van Sinderen, D. Lytic Infection of Lactococcus lactis by Bacteriophages Tuc2009 and c2 Triggers Alternative Transcriptional Host Responses. *Appl. Environ. Microbiol.* **2013**, *79*, 4786–4798, doi:10.1128/AEM.01197-13.
27. Chaikeeratisak, V.; Nguyen, K.; Egan, M.E.; Erb, M.L.; Vavilina, A.; Pogliano, J. The Phage Nucleus and Tubulin Spindle Are Conserved among Large Pseudomonas Phages. *Cell Rep.* **2017**, *20*, 1563–1571, doi:10.1016/j.celrep.2017.07.064.
28. Chaikeeratisak, V.; Nguyen, K.; Khanna, K.; Brilot, A.F.; Erb, M.L.; Coker, J.K.C.; Vavilina, A.; Newton, G.L.; Buschauer, R.; Pogliano, K.; et al. Assembly of a nucleus-like structure during viral replication in bacteria. *Science* **2017**, *355*, 194–197, doi:10.1126/science.aal2130.
29. Mastronarde, D.N. Automated electron microscope tomography using robust prediction of specimen movements. *J. Struct. Biol.* **2005**, *152*, 36–51, doi:10.1016/j.jsb.2005.07.007.
30. Kremer, J.R.; Mastronarde, D.N.; McIntosh, J.R. Computer Visualization of Three-Dimensional Image Data Using IMOD. *J. Struct. Biol.* **1996**, *116*, 71–76, doi:10.1006/jsbi.1996.0013.
31. Introduction to 3dmod, Version 4.9. Available online: https://bio3d.colorado.edu/imod/doc/3dmodguide.html (accessed on Jul 28, 2019).
32. Fokine, A.; Battisti, A.J.; Bowman, V.D.; Efimov, A. V.; Kurochkina, L.P.; Chipman, P.R.; Mesyanzhinov, V. V.; Rossmann, M.G. Cryo-EM Study of the Pseudomonas Bacteriophage φKZ. *Structure* **2007**, *15*, 1099–1104, doi:10.1016/j.str.2007.07.008.
33. Campbell, E.A.; Korzheva, N.; Mustaev, A.; Murakami, K.; Nair, S.; Goldfarb, A.; Darst, S.A. Structural Mechanism for Rifampicin Inhibition of Bacterial RNA Polymerase. *Cell* **2001**, *104*, 901–912, doi:10.1016/S0092-8674(01)00286-0.
34. Ceyssens, P.-J.; Minakhin, L.; Van den Bossche, A.; Yakunina, M.; Klimuk, E.; Blasdel, B.; De Smet, J.; Noben, J.-P.; Blasi, U.; Severinov, K.; et al. Development of Giant Bacteriophage ϕKZ Is Independent of the Host Transcription Apparatus. J. Virol. 2014, 88, 10501–10510, doi:10.1128/JVI.01347-14.
35. Lewin, B. *Genes IX*; 9th ed.; Jones & Bartlett Publishers: USA, Sudbury, MA, 2007.
36. Wu, W.; Thomas, J.A.; Cheng, N.; Black, L.W.; Steven, A.C. Bubblegrams Reveal the Inner Body of Bacteriophage ϕKZ. *Science* **2012**, *335*, 182–182, doi:10.1126/science.1214120
37. Erb, M.L.; Kraemer, J.A.; Coker, J.K.C.; Chaikeeratisak, V.; Nonejuie, P.; Agard, D.A.; Pogliano, J. A bacteriophage tubulin harnesses dynamic instability to center DNA in infected cells. *Elife* **2014**, *3*, doi:10.7554/eLife.03197.
38. Loiko, N.; Danilova, Y.; Moiseenko, A.; Kovalenko, V.; Tereshkina, K.; El-Registan, G.; Sokolova, O.; Krupyanskii, Y. Morphological peculiarities of DNA-protein complexes in dormant Escherichia coli cells, subjected to prolonged starvation Condensation of DNA in dormant cells of Escherichia coli. *bioRxiv*, doi:10.1101/2020.03.27.011494.
39. Frenkiel-Krispin, D.; Minsky, A. Nucleoid organization and the maintenance of DNA integrity in E. coli, B. subtilis and D. radiodurans. *J. Struct. Biol.* **2006**, *156*, 311–319, doi:10.1016/j.jsb.2006.05.014.
40. Almirón, M.; Link, A.J.; Furlong, D.; Kolter, R. A novel DNA-binding protein with regulatory and protective roles in starved Escherichia coli. *Genes Dev.* **1992**, *6*, 2646–2654.
41. Minsky, A.; Shimoni, E.; Frenkiel-Krispin, D. Stress, order and survival. *Nat. Rev. Mol. Cell Biol.* **2002**, *3*, 50–60, doi:10.1038/nrm700.
42. Hanninen, A.-L.; Bamford, D.H.; Bamford, J.K.H. Assembly of Membrane-Containing Bacteriophage PRD1 Is Dependent on GroEL and GroES. *Virology* **1997**, *227*, 207–210, doi:10.1006/viro.1996.8308.
43. De Smet, J.; Zimmermann, M.; Kogadeeva, M.; Ceyssens, P.-J.; Vermaelen, W.; Blasdel, B.; Bin Jang, H.; Sauer, U.; Lavigne, R. High coverage metabolomics analysis reveals phage-specific alterations to Pseudomonas aeruginosa physiology during infection. *ISME J.* **2016**, *10*, 1823–1835, doi:10.1038/ismej.2016.3.

Preprints (www.preprints.org) | NOT PEER-REVIEWED | Posted: 28 August 2020 doi:10.20944/preprints202008.0633.v1

44. Moiseenko, A.; Loiko, N.; Tereshkina, K.; Danilova, Y.; Kovalenko, V.; Chertkov, O.; Feofanov, A. V.; Krupyanskii, Y.F.; Sokolova, O.S. Projection structures reveal the position of the DNA within DNA-Dps Co-crystals. *Biochem. Biophys. Res. Commun.* **2019**, *517*, 463–469, doi:10.1016/j.bbrc.2019.07.103.
45. Frenkiel-Krispin, D.; Ben-Avraham, I.; Englander, J.; Shimoni, E.; Wolf, S.G.; Minsky, A. Nucleoid restructuring in stationary-state bacteria. *Mol. Microbiol.* **2004**, *51*, 395–405, doi:10.1046/j.1365-2958.2003.03855.x.
46. Wolf, S.G.; Frenkiel, D.; Arad, T.; Finkel, S.E.; Kolter, R.; Minsky, A. DNA protection by stress-induced biocrystallization. *Nature* **1999**, *400*, 83–5, doi:10.1038/21918.